Evaluation of the energy efficiency of conversion in microwave discharges using a reaction kinetics model

Plasma sources science and technology / **Institute of Physics** - ISSN 0963-0252 - 24(2015), 015024

DOI: http://dx.doi.org/doi:10.1088/0963-0252/24/1/015024

Handle: http://hdl.handle.net/10067/1222430151162165141

Evaluation of the energy efficiency of CO_2 conversion in microwave discharges using a reaction kinetics model

Tomáš Kozák and Annemie Bogaerts

Department of Chemistry, Research group PLASMANT, University of Antwerp, Universiteitsplein 1, B-2610 Antwerp, Belgium

E-mail: annemie.bogaerts@uantwerpen.be

Abstract. We use a zero-dimensional reaction kinetics model to simulate CO_2 conversion in microwave discharges where the excitation of the vibrational levels play a significant role in the dissociation kinetics. The model includes a description of the CO_2 vibrational kinetics, taking into account state-specific VT and VV relaxation reactions and the effect of vibrational excitation on other chemical reactions. The model is used to simulate a general tubular microwave reactor, where a stream of CO_2 flows through a plasma column generated by microwave radiation. We study the effects of the internal plasma parameters, namely the reduced electric field, electron density and the total specific energy input, on the CO_2 conversion and its energy efficiency. We report the highest energy efficiency (up to 30 %) for a specific energy input in the range $0.4 - 1.0\,\mathrm{eV/molecule}$ and a reduced electric field in the range $50 - 100\,\mathrm{Td}$ and for high values of the electron density (ionization degree greater than 10^{-5}). The energy efficiency is mainly limited by the VT relaxation which contributes dominantly to the vibrational energy losses and contributes also significantly to the heating of the reacting gas. The model analysis provides useful insight into the potential and limitations of CO_2 conversion in microwave discharges.

1. Introduction

The growing concentration of greenhouse gases becomes a concern for the climate change[1]. Therefore, the idea of their conversion into useful chemicals has recently become very actual. Using the (at certain moments abundant) renewable energy to convert CO_2 and H_2O into carbon-containing liquid fuels would provide a way to store the renewable energy into so-called "solar fuels" and decrease CO_2 emissions at the same time.

One of the challenges is to maximize the energy efficiency of the first step in the process – the CO_2 dissociation. In the 1970's and 1980's, CO_2 dissociation by plasmas has been extensively studied both theoretically and experimentally[2, 3, 4, 5, 6]. It was concluded that microwave discharges provide the highest possible energy efficiency due to a combination of relatively high electron density and low reduced electric field which favour the excitation of the asymmetric mode vibrational levels of CO_2, and thus enhance the dissociation even at low gas temperature[5]. This efficient dissociation channel is in fact a combination of several reaction steps – excitation by electrons, VT and VV relaxation and dissociation of the excited vibrational levels stimulated by collisions with other molecules. Moreover, a whole spectrum of vibrational levels is involved in these reactions.

More recently, new experiments in microwave discharges are being carried out to evaluate the possibility of using this technology for CO_2 conversion[7, 8, 9, 10]. These experiments differ in the geometry of the reactor, gas pressure, gas flow and specific energy input used. Due to the complex multi-step nature of the dissociation process, with many vibrational levels involved, not all aspects of the conversion mechanism in these discharges are well understood yet. A computer simulation can provide the data that are difficult to measure, such as the densities of individual vibrational levels, reaction rates, etc., and it can help to determine the optimal process conditions for maximizing the energy efficiency.

Building an accurate model for a specific plasma reactor with a complex CO_2 chemistry is a big task. As a first step, we focus on the chemical kinetics of CO_2 in non-equilibrium discharges with special attention to the vibrational levels which, as mentioned earlier, play an important role in an energy-efficient conversion process. Recently, we have published a paper presenting the reaction kinetics model for the CO_2 conversion in non-equilibrium plasmas[11]. We have shown that vibrational levels of CO_2 are indeed very important in a microwave discharge as opposed to a dielectric barrier discharge. Because of the high activation energy barrier for the dissociation reaction $CO_2 \longrightarrow CO + O$ (5.5 eV), the population of the highly excited vibrational levels must be sufficiently high to obtain significant dissociation. We have used the model to calculate the vibrational distribution function of CO_2 and the overall CO_2 conversion and its energy efficiency under given process conditions.

In the present paper, we use the reaction kinetics model to study in more detail the CO_2 conversion in a moderate-pressure microwave discharge under various discharge conditions. A distinct improvement compared to the previous model[11] is the addition of an energy conservation equation for the neutral gas, which is used to calculate the gas temperature evolution in the discharge. We define here the electron density and the reduced electric field as the internal plasma parameters and the specific energy input to describe the overall energy delivered to the reacting gas. We study the effect of these parameters on the energy efficiency of the CO_2 conversion. Moreover, we analyze the time evolution of the gas and vibrational temperature in the discharge

and we identify the main factors limiting the energy efficiency. Thus, this paper provides important details about the reaction kinetics in microwave discharges and gives recommendation for the optimal process conditions.

The paper is organized as follows. In section 2, the model equations, model species and reactions are described and the corresponding (thermodynamic) data are specified. The results part (section 3) is divided into three subsections. In the first, the effects of the specific energy input, reduced electric field and electron density on the conversion and energy efficiency are discussed. In the second, the evolution of the gas temperature and its effect the CO_2 conversion and energy efficiency are evaluated. Finally, in the third subsection, we discuss the vibrational energy losses caused by individual reactions and how this affects the energy efficiency of the conversion process. These detailed discussions will contribute to a better understanding of the results presented in the first subsection. Finally, a conclusion is presented in section 4.

2. Description of the model

A reaction kinetics model was developed to simulate the state-to-state vibrational kinetics of CO_2 in a non-equilibrium plasma. The model can be characterized as a zero-dimensional model. Mathematically, it is expressed by a set of coupled ordinary differential equations of the form

$$\frac{\mathrm{d}n_i}{\mathrm{d}t} = \sum_j \left[(a_{ij}^{\mathrm{R}} - a_{ij}^{\mathrm{L}}) k_j \prod_l n_l^{\mathrm{L}} \right] , \tag{1}$$

where n_i is the density of species i, a_{ij}^{R} and a_{ij}^{L} are the right-hand side and left-hand side stoichiometric coefficients of species i in the reaction j, k_j is the reaction rate constant and n_l^{L} is the density of the lth reactant of reactions j. The energy equation for the gas translational temperature, T_{g}, is included in the form

$$N \frac{\gamma k}{\gamma - 1} \frac{\mathrm{d}T_{\mathrm{g}}}{\mathrm{d}t} = P_{\mathrm{e,el}} + \sum_j R_j \Delta H_j - P_{\mathrm{ext}} , \tag{2}$$

where $N = \sum n_i$ is the total gas density, $\gamma = c_p/c_v$ is the ratio of specific heats, k is the Boltzmann constant, $P_{\mathrm{e,el}}$ is the gas heating power density due to elastic electron–neutral collisions, R_j is the rate of reaction j, ΔH_j is the heat released (or consumed, when the value is negative) in the reaction and P_{ext} is the heat loss due to energy exchange with the surroundings. Equation (2) can be derived from a general energy conservation equation[12]

$$\rho \frac{\mathrm{D}h}{\mathrm{D}t} = \frac{\mathrm{D}p}{\mathrm{D}t} + \frac{\partial Q}{\partial t} - \nabla \boldsymbol{q} + \Phi , \tag{3}$$

by assuming isobaric conditions and neglecting the spatially dependent heat conduction term, $\nabla \boldsymbol{q}$, and the viscosity heating term, Φ. For an ideal gas, the specific enthalpy change is expressed as $\mathrm{d}h = c_p \mathrm{d}T$, where $c_p = \gamma/(\gamma - 1)k/m$ and m is the species mass. For a mixture of ideal gases, γ is calculated at any given time using the known species densities, n_i, and the specific heat ratios of individual species, γ_i, according to the formula

$$N \frac{\gamma}{\gamma - 1} = \sum_i n_i \frac{\gamma_i}{\gamma_i - 1} . \tag{4}$$

Equations (1) and (2) are also coupled with the Boltzmann equation which is solved for the electron energy distribution function (EEDF). Energy is supplied to the plasma electrons by an external electric field (specified by the reduced electric field E/N and by the reduced frequency ω/N, in case of an AC field). We use an existing code ZDPlasKin[13] which features an interface for description of the plasma species and reactions, a solver for the set of differential equations (1) and (2) and a Boltzmann equation solver BOLSIG+[14].

This model is used to simulate CO_2 decomposition in a microwave discharge. Because the model is zero-dimensional, we can only describe a reactor with a simple geometry and we have to make certain approximations which are discussed in the following paragraphs.

An example of such a simple reactor setup was presented in a recent experimental work of Silva et al.[10]. It consists of the dielectric tube and a waveguide that leads the microwaves perpendicular to the tube. A plasma column is formed in the tubular reactor. The plasma is generated by the electric field and, at the same time, supports the propagation of the waves along the reactor. The plasma column length depends on the process conditions such as the geometry and the dielectric material, gas pressure and input power. A self-consistent simulation of the discharge is beyond the scope of this paper. By using the zero-dimensional model, we focus specifically on the reaction kinetics and the gas flow along the reactor axis is described in a one-dimensional approximation. Therefore, we assume all variables are uniform in the radial direction and we also neglect diffusion and heat conduction along the reactor axis, which we believe is reasonable for the relatively high pressure used (100 Torr) and short residence times ($< 10^{-3}$ s); see the input parameters used in section 3. We also assume quasineutrality of the plasma in the simulated volume, the effects of sheaths near the dielectric walls are neglected. For these reactor dimensions and the sub-atmospheric pressure of the gases, we can neglect the effects of viscosity and assume the pressure is constant everywhere. Under these assumption, the particle density and total energy conservation equations for a steady state reduce to the model equations presented above.

The velocity of the gas, v, in the reactor is given by the mass conservation law as

$$v = \frac{Q_m}{\rho A}\,, \tag{5}$$

where Q_m is the mass flow rate (in kgs^{-1}), $A = \pi R^2$ is the reactor cross section area and $\rho = \sum_i n_i m_i$ is the gas mass density. As the gas temperature increases, the particle densities decrease in order to maintain the constant pressure and the gas velocity increases to maintain the constant mass flow. Equation (1) does not account for the gas expansion at constant pressure (as it is implemented in ZDPlasKin with respect to the assumption of a fixed simulation volume). Therefore, at each time step of the simulation, the gas pressure is calculated from the actual particle densities and gas temperature, and the particle densities are then corrected to maintain the constant pressure.

Assuming that heat conduction is the predominant cooling mechanism and that the reactor walls are kept at a constant temperature T_w, the heat loss term in eq. (2) is given as[15]

$$P_\mathrm{ext} = \frac{8\lambda(T_\mathrm{g})}{R^2}(T_\mathrm{g} - T_\mathrm{w})\,, \tag{6}$$

where λ is the gas thermal conductivity and R is the reactor radius. For simplicity, we use the thermal conductivity of CO_2, which is the dominant gas in our simulations. The experimental data compiled by Vesovic et al.[16] in the temperature range $200 - 1350\,\mathrm{K}$ were fitted by a linear function to obtain $\lambda = (0.071T_\mathrm{g} - 2.33) \times 10^{-5}\,\mathrm{Wcm^{-1}K^{-1}}$.

The plasma conditions are represented by the electron density and the electric field in each position in the reactor, which can be uniquely represented in time as the gas flows through the discharge region. The characteristic features of a microwave discharge are a continuous input of power through an alternating electric field with a relatively low reduced electric field ($10 - 100\,\mathrm{Td}$), resulting in an electron temperature of around $1\,\mathrm{eV}$[17]. As our model is not self-consistent, we set the internal plasma parameters directly rather than the total power deposition. This allows us to see the uncoupled effects of these parameters on the reaction kinetics, as we believe this gives us a better understanding of the experimental results. Also, it makes the conclusions more easily transferable to other discharge conditions.

The simulation can be divided in two phases – power deposition and relaxation. In the first phase, electrons are energized by the electric field and they activate the other plasma species. This corresponds to the gas passing through the plasma column. For simplicity, the reduced electric field and the electron density are introduced as constant values in this phase. In the second phase, the power deposition goes to zero (which is translated in the simulation as the electron density going to zero), and the reacting species are given time to relax back to equilibrium. We are aware that by fixing the electron density, we are changing the kinetics bound to the electron impact reactions, and that by setting the electron density to zero for the relaxation phase, we neglect the relaxation of the electron distribution function in the afterglow [18]. This should be certainly considered in a detailed model where the coupling with the electromagnetic field propagation in the plasma is calculated. On the other hand, this simple model setup allows us to study the general conversion trends as functions of the electron density and the reduced electric field with a significantly lower computational demand.

The total energy input per one CO_2 molecule entering the reactor is called the specific energy input SEI and it can be expressed as

$$\mathrm{SEI} = \frac{P}{Q_N(0)} = \frac{P m_\mathrm{avg}(0)}{Q_m}\,, \tag{7}$$

where P is the total power absorbed by the plasma electrons , $Q_N(0) = Q_m/m_\mathrm{avg}(0)$ is the gas flow rate at the reactor inlet and m_avg is the average mass of the species at the reactor inlet. When the power is expressed in $\mathrm{eV}s^{-1}$ and the gas flow rate in s^{-1}, we obtain SEI in the typical units of eV/molecule.

The total power absorbed in the plasma column, P, can be evaluated as

$$P = \int_0^{t_\mathrm{r}} P_\mathrm{e,tot} A v \mathrm{d}t = \int_0^{t_\mathrm{r}} \frac{P_\mathrm{e1}}{N}(n_i, \frac{E}{N}) n_\mathrm{e} Q_N \mathrm{d}t\,, \tag{8}$$

where t_r is the length of the power deposition phase, i.e. the residence time of the gas within the plasma, $P_\mathrm{e,tot}$ is the total power density absorbed by electrons and P_e1 is the power absorbed by one electron which is obtained in the form P_e1/N from the solution of the Boltzmann equation. Equations (7) and (8) indicate that by specifying the internal plasma parameters and the SEI, we constrain the residence time, t_r. We

Table 1. Summary of all species included in the model. The numbers between brackets indicate the number of excited levels taken into account.

Neutral ground states	CO_2, CO, O_2, O_3, O, C_2O, C, C_2
Vibrational levels	CO_2(25), CO(63), O_2(4)
Electronic states	CO_2(2), CO(4), O_2(2)
Charged species	CO_2^+, e

can also notice from (8) that when the electron density is constant in time (as assumed in this work), the total power is proportional to the electron density value used in the calculation. Moreover, in the first approximation, i.e. when E/N is constant and the gas composition is not changing very much, the total power is proportional to the product of the electron density and the residence time. Consequently, taking into account (7), the residence time is inversely proportional to the electron density for a fixed SEI. The total simulation time, t_{end}, is set to 0.1 s, which is sufficient for the relaxation of the vibrational levels and the gas temperature.

2.1. Reacting species and their chemistry

The species and reactions used in this work are based on our previous work[11]. We have found that the dissociation of CO_2 is strongly influenced by the population of highly excited vibrational levels, which are determined mainly by electron impact vibrational excitation and by the VT and VV relaxation of the CO_2 vibrational levels. Compared to the previous paper[11], we have reduced the reaction chemistry by omitting all charged species (except for electrons and CO_2^+ ions), which play a minor role in the kinetics of the neutral species and, as mentioned above, we simply set the electron density to a given value.

The species included in the model are summarized in table 1. For CO_2, CO and O_2, we have included several vibrational levels and electronically excited levels. The vibrational levels of CO_2 used in the model are shown in figure 1. We use the four lowest effective symmetric mode levels (denoted by letters) and 21 asymmetric mode levels (denoted by numbers) up to the dissociation limit of the molecule. We have further extended the number of CO vibrational levels to 63, in order to cover also the whole range of energies up to the dissociation energy.

We have used only a few electronic excited states of CO_2, CO and O_2, see Table 1, primarily to account for the electron energy losses in their excitation, see Table A1. Radiative and collision-induced quenching of these states is included in the model, using the data [19] for CO and [20] for O_2. Due to the lack of data, for CO_2, we used quenching rate constants of the same order of magnitude as for CO. As will be discussed a posteriori in section 3, under the conditions investigated, most of the electron energy goes to the vibrational levels and, therefore, the limited description of the electronic excited states does not affect the calculated CO_2 conversion.

The reactions used in the model are of three types: electron impact reactions, heavy particle reactions involving change of vibrational energy and heavy particle chemical reactions (formation of new species), see tables A1, A2 and A3, respectively. Surface reactions on the reactor walls are not taken into account in the model. Due to the high pressure of 100 Torr used in the present calculations, the characteristic diffusion time (estimated to be in the order of 10^{-2} s for the gas temperature of 1000 K) is much longer than the residence time in the plasma, see Figure 5 below.

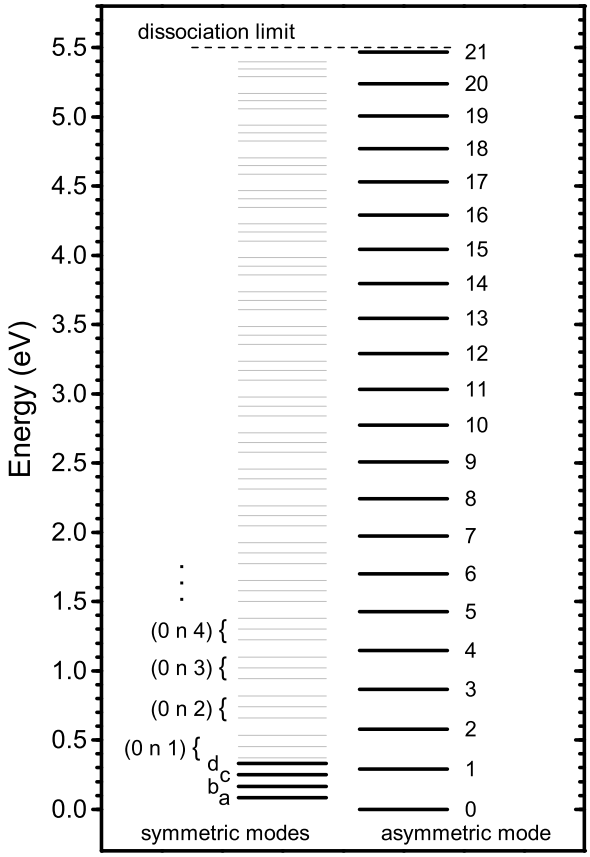

Figure 1. Effective energy levels of CO_2 included in the model (black lines), i.e., 4 symmetric mode levels (denoted by letters), 21 asymmetric mode levels (denoted by numbers from 1 to 21) and the CO_2 ground state (denoted by 0). Adopted from [11] with permission from Institute of Physics.

Therefore, the effect of the wall reactions on the CO_2 conversion in the plasma is limited by the slow diffusion and can be neglected at the conditions used. In the next paragraphs, we will have a closer look at the reactions used, however, for even more detailed information about the reactions and the rate constants used, see [11].

The electron impact reactions (table A1) are given in the form of a cross section database that is passed to the Boltzmann equation solver. Because we have omitted charged species such as CO^+, O^+ and O^- from the model, the reactions which result in the formation of these ions are not taken into account in the particle balance equations (eq. (1)), nevertheless, these reactions are included in the cross section database in order to calculate the EEDF correctly. Due to the lack of cross section data for reactions with the vibrational excited states, we have modified the cross sections for the ground states based on two basic rules. For dissociation and dissociative ionization reactions, we have lowered the energy threshold by the vibrational energy of the reacting state, whereas for the other reactions we have used the same cross

sections as for the ground state; see the notes in table A1. Laporta et al. recently calculated a complete set of state-to-state cross sections for CO [21]. Nevertheless, we used the above mentioned approach to be consistent with the treatment of the CO_2 molecule, for which such complete data are not yet available. The Boltzmann equation solver is called automatically during the run of the ZDPlasKin code whenever the input parameters or the gas composition changes significantly.

The heavy particle reactions in tables A2 and A3 are specified by temperature-dependent rate constants. The vibrational energy exchange reactions in table A2 include three types of reactions: VT relaxation (V1 – V4), intermode VV relaxation which represents vibrational energy exchange among the symmetric and asymmetric mode levels of CO_2 (V5) and VV relaxation between CO_2 and CO molecules (V6 – V8). VT relaxation is the main process responsible for the decrease of vibrational energy stored in the molecules. The VV relaxation among CO_2 levels (V6) is almost resonant, i.e. little vibrational energy is lost to translation, and it is responsible for redistribution of the vibrational energy in the asymmetric mode. This reaction leads to the population of high-energy levels (Treanor distribution)[22]. For all reactions, only single-quantum transitions are taken into account. The reaction rate constants for the lowest vibrational levels were obtained from the given references. For the higher vibrational levels, a scaling law based on the Schwartz-Slawsky-Herzfeld (SSH) theory[23] was used to calculate the rate constants. We have calculated state-specific rate constants in the temperature range $300 - 1000\,\mathrm{K}$ and used nonlinear curve fitting to obtain a temperature-dependent expression for each reaction in the form $AT_\mathrm{g}^n \exp(-BT_\mathrm{g}^{-1/3} + CT_\mathrm{g}^{-2/3})$. The rate constants for backward reactions were calculated using the detailed balance principle. The vibrational energy difference in VT, VV' and VV reactions contribute to the gas heating through ΔH_j in (2).

The chemical reactions in table A3 represent the reactions of the ground states as well as all the vibrational excitation states. For the vibrational levels, the rate constants are determined by the Fridman–Macheret α-model[24, 17] which assumes that the activation energy of a reaction is lowered by the vibrational energy of the reacting species multiplied by an effectiveness parameter α. This parameter is assumed to be 1 for strongly endothermic reactions, such as (N1) and (N9), and 0.5 for thermoneutral reactions such as (N2) and (N4). Therefore, an excited molecule of CO_2 with vibrational energy close to the dissociation limit is easily dissociated through reactions (N1) and (N2), which are the most important reactions for CO_2 dissociation in microwave discharges, as we have shown in our previous paper[11]. The heat released or consumed in a reaction, ΔH_r, appears as a source term in the energy conservation equation (2). Naturally, any extra vibrational energy lost in a reaction is added to this value. We assume that in dissociation reactions, all vibrational energy is transformed in the translational energy of the reaction products.

Regarding the energy conservation equation, we have to provide the specific heat ratio for each species, γ_i, that is used to calculate the total specific heat ratio of the gas mixture, γ. It is important to bear in mind, that the vibrational levels are simulated by separate species in the model, so we have to take into account only the heat capacity due to translational and rotational degrees of freedom and, in case of CO_2, the heat capacity due to the symmetric vibrational modes which are not resolved by individual model species. Therefore, the required specific heat ratios at room temperature and above can be well approximated by taking into account the classical energy partitioning between the translational and rotational degrees of freedom, which gives a value of 1.67 for atoms and 1.40 for diatomic molecules. For O_3, we used a value of 1.27 taken

Table 2. Fitting constants for calculating the specific heat capacity of CO_2 due to translational, rotational and symmetric mode vibrational degrees of freedom.

Temperature	$300 - 1200\,\mathrm{K}$	$1200 - 3000\,\mathrm{K}$
A	369.4	1327
B	1845	−53.85
C	−1429	31.52
D	401.2	−5.841
E	3.664	−109.6

at 300 K[25]. For CO_2, which is the most important species in our simulation, we have to take into account the heat capacity of the symmetric mode levels. We have generated a set of effective symmetric mode levels with energies $\varepsilon_n = n \times 0.0828\,\mathrm{eV}$ and degeneracies that reflect the number of levels in the symmetric stretch and symmetric bend modes. For this set, we have calculated the specific heat capacity of the effective symmetric vibrational mode as

$$C_{\mathrm{vib}}(T_{\mathrm{g}})\,[\mathrm{JK}^{-1}/\mathrm{molecule}] = \frac{\mathrm{d}\overline{\varepsilon}(T_{\mathrm{g}})}{\mathrm{d}T_{\mathrm{g}}}\,, \tag{9}$$

where $\overline{\varepsilon}(T_{\mathrm{g}})$ is the average vibrational energy of the symmetric mode levels at a given equilibrium temperature T_{g}. The total heat capacity for translational, rotational and symmetric vibrational degrees of freedom was obtained by adding a constant so that the resulting value is equal to the experimental heat capacity at 300 K. Indeed, at this temperature, the excitation of asymmetric mode levels is negligible. The result can be expressed (using the same polynomial model as in [25]) as

$$c_p\,[\mathrm{Jkg}^{-1}\mathrm{K}^{-1}] = A + Bt + Ct^2 + Dt^3 + Et^{-2}\,, \qquad t = T[K]/1000\,, \tag{10}$$

with the fitting coefficients given in table 2.

We should point out that the use of the temperature-dependent c_p for CO_2 in (2) is valid when the electron induced transitions of the symmetric levels are slower than the vibrational relaxation of these levels, i.e., the distribution of the symmetric mode levels is not disturbed by the significantly warmer electrons. This condition is critical especially for the lowest levels for which the vibrational relaxation is the slowest and electron excitation is the fastest. For the pressure of 100 Torr and the CO_2(Va) level, we can estimate the collision frequency $Nk_{\mathrm{VT}} \approx 2 \times 10^4\,\mathrm{s}^{-1}$ for vibrational relaxation and $5 \times 10^{-9} n_{\mathrm{e}}\,\mathrm{s}^{-1}$ for electronic excitation. Therefore, the condition that vibrational relaxation is faster than electronic excitation is valid approximatelly for $n_{\mathrm{e}} < 4 \times 10^{12}\,\mathrm{cm}^{-3}$. That is why we have included the lowest symmetric mode levels as separate species in the model. For the higher symmetric mode levels, the electron induced reactions tend to be slower due to smaller reaction rate constants (in the case of an excitation from the ground state) and lower density of the reacting species, in the case of a step-by-step excitation from a lower level). Moreover, the relaxation rate constants are increasing as the level number increases. Therefore, we are confident that this approximation does not bring a significant error to the temperature calculations (compared to the other assumption of the model) even for electron densities higher than $10^{12}\,\mathrm{cm}^{-3}$.

2.2. Characteristics calculated from the simulation results

For each simulation run, we obtain the time evolution of the gas temperature and the densities of individual species, including all vibrational levels. Here, we define several important characteristics that are calculated from these raw results and are used frequently in the next section.

The conversion of CO_2 is the fraction of CO_2 molecules that are decomposed as they flow through the reactor. At each time, the conversion is given as

$$X(t) = \left(1 - \frac{n_{CO_2}(t)v(t)}{n_{CO_2}(0)v(0)}\right) \cdot 100\,\%\,, \tag{11}$$

where n_{CO_2} is the total CO_2 density and v is the gas velocity as defined by eq. (5). The value in the denominator is the CO_2 inlet flow density, Q_N/A. When we speak about the conversion of CO_2 under certain conditions, we mean the total conversion at the end of the simulation, $X(t_{\mathrm{end}})$. The energy efficiency of the CO_2 conversion is calculated as

$$\eta = X\frac{2.93}{\mathrm{SEI}}\,, \tag{12}$$

where 2.93 eV is the energy cost of splitting one CO_2 molecule into CO and 1/2 O_2 and the specific energy input (SEI) is defined by eq. (7) above.

Finally, the vibrational temperature gives us an indication about the amount of vibrational excitation in a molecule. The vibrational temperature is commonly defined as[22]

$$T_{\mathrm{v}} = -\frac{E_1}{\ln\frac{n_1}{n_0}}\,, \tag{13}$$

where E_1 is the energy of the first vibrational level, n_1 is its density and n_0 is the ground state density. This equation is applied in the same way to the asymmetric mode levels of CO_2 and to the vibrational levels of CO.

3. Results and discussion

We use the model described above to study the effect of the specific energy input, the reduced electric field and the electron density on the conversion of CO_2. As our basic working conditions, we chose a gas pressure of 100 Torr, which is mentioned as being the optimum value for energy-efficient CO_2 splitting[17]. The electric field frequency is kept at the typical value of 2.45 GHz for all simulations. Initially, the gas temperature is 300 K, but during the simulation it rises, as will be shown below. However, to investigate the effect of this rising gas temperature, we have also performed simulations for a fixed gas temperature of 300 K. The wall temperature, T_{w}, is also kept at 300 K, which may be achieved by cooling of the reactor walls. We performed several simulations with different values of the electron density in the range 10^{11} to $10^{14}\,\mathrm{cm}^{-3}$, reduced electric field in the range $10 - 100$ Td and specific energy input in the range $0 - 2$ eV/molecule. Typically, we only varied one parameter at a time. For the parameters that are kept constant, we used the values $10^{13}\,\mathrm{cm}^{-3}$, 50 Td and 1 eV/molecule, which give rise to an energy efficiency close to the maximum value observed in this series of calculations.

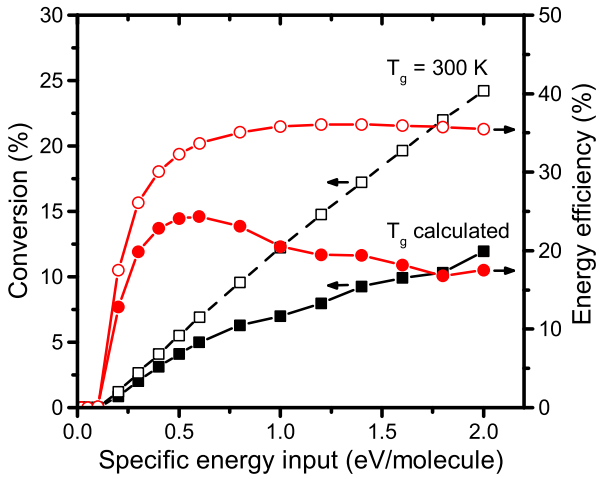

Figure 2. Conversion of CO_2 and its energy efficiency as a function of the specific energy input, with $p = 100$ Torr, $E/N = 50$ Td and $n_e = 10^{13}$ cm^{-3}. The results are shown for both a self-consistently calculated gas temperature (full symbols) and a gas temperature fixed at 300 K (empty symbols).

3.1. Effects of the specific energy input, reduced electric field and electron density

Figure 2 shows the conversion and energy efficiency as a function of the specific energy input (SEI) at constant values of gas pressure, E/N and electron density, both at a constant gas temperature of 300 K and at the gas temperature self-consistently calculated by the model. The conversion is practically zero below a critical SEI around 0.2 eV/molecule and then it starts rising with increasing SEI. Also the energy efficiency is zero below a SEI of 0.2 eV/molecule, and a maximum is reached at 0.6 eV/molecule. These results are in a very good agreement with the theoretical and experimental results of Rusanov and Fridman[5]. In our case, however, the maximum energy efficiency (i.e., 36 % when assuming a constant gas temperature of 300 K and 25 % in case of the self-consistently calculated gas temperature) is not as high as that presented in [5], where energy efficiencies up to 80 % were reported. Further in this paper, and especially in section 3.3, we will discuss the major effects that limit the maximum energy efficiency in our case.

Also mentioned above, we compare in figure 2 the model results with a varying gas temperature with those where the gas temperature was fixed at 300 K. The latter corresponds to the situation of our previous paper[11] where the simulation code used did not allow us to calculate the gas temperature. We can see that the trends are very similar, but a significantly lower energy efficiency is obtained when the gas temperature is allowed to increase. This is primarily due to the temperature dependence of the VT relaxation rate constants, as will be analyzed in more detail later in this paper. Furthermore, we notice that for the constant temperature case, the conversion increases practically linearly with the SEI, whereas in the variable temperature case, the conversion increases less then linearly. This causes the much more prominent peak shape of the energy efficiency, see (11), which has also been shown in the literature[17]

In order to understand better the time scales of the processes taking place during

the splitting of CO_2, we show in figure 3 the time dependent analysis for the case with SEI = 0.6 eV/molecule (cf. figure 2). The top panel shows the increase of the SEI in time, until it reaches the prescribed value at the residence time of $t_r = 1.4 \times 10^{-5}$ s (i.e., when the gas has passed the plasma column; see vertical dashed line). The red curve shows the time evolution of the CO_2 conversion. We can notice that the conversion starts increasing at around 4×10^{-6} s when the SEI is around 0.2 eV/molecule. This corresponds also with the results shown in figure 2. Clearly, below this SEI, the density of the high vibrational levels of CO_2 is not yet high enough for significant dissociation, as was also demonstrated in [11]. After the gas has passed the plasma column (i.e., after t_r), the conversion saturates on a very short timescale (i.e., order of 10^{-5} s). Until the end of the simulation, the conversion slightly decreases, which is most likely caused by reverse reactions, e.g. (N3), (N4) and (N6) in table A3, which are boosted by the increased gas temperature, see the middle panel of figure 3.

The middle panel shows the evolution of the electron, gas and vibrational temperatures of CO_2 (asymmetric mode) and CO, see (13). The electron temperature is approximately constant at around 0.4 eV (or 4500 K) during the simulation. At this moment, we have to remind the reader that the electron temperature is calculated by Boltzmann equation solver using the local field approximation for the given value of E/N. Therefore, the model cannnot describe the decrease of the electron temperature towards gas temperature in the afterglow when (in reality) the electric field goes to zero. In the simulation, we terminate the plasma activation phase by setting the electron density to zero at $t = t_r$, therefore all processes involving electrons are suppressed for $t > t_r$. The slight changes of electron temperature result from the changes in the gas composition, corresponding to the changes in the population of the lowest CO_2 vibrational levels. The relatively low electron temperature corresponds to the reduced electric field value of 50 Td. This is close to optimal for exciting the asymmetric mode vibrational levels, see figure 4 below. However, it should be noted, that due to the fixed electron density, our simulation is not self-consistent and we expect that higher E/N and higher electron temperatures might be necessary to generate and sustain the electron density.

The vibrational temperature of CO_2 and CO increases from the very beginning of the simulation, as a result of excitation by electrons. Nevertheless, we must keep in mind that at the beginning, there are practically no CO molecules, so the absolute population of the CO vibrational levels will be limited. The vibrational temperatures reach values of several thousand Kelvin. The conversion of CO_2 starts to increase when the CO_2 vibrational temperature reaches approximately 2500 K (cf. top and middle panel). At around 10^{-5} s, the gas temperature starts to increase as well, mainly as a result of VT relaxation reactions. After the electron density is set to zero at t_r, i.e. when the gas has passed the plasma column, the vibrational temperatures quickly decrease on the time scale of 10^{-4} s. The gas temperature continues to increase due to the VT relaxation reactions until all temperatures (except the electron temperature) are in equilibrium. The gas temperature then continues to decrease slowly as a result of the heat exchange with the reactor walls, which is a much slower process on the time scale of approximately 10^{-1} s.

The bottom panel shows the time evolution of the densities of neutral species. In this graph, the densities of CO_2, CO and O_2 represent the total densities of these species, including also the electronic and vibrationally excited levels. Again, we can see an abrupt increase of the CO and O species which are produced by reaction (N1), when the CO_2 vibrational temperature is high enough, indicating that the CO_2

conversion indeed occurs as soon as the population of the higher CO_2 vibrational levels is sufficiently high. This reaction is followed by reaction (N2), which converts O into O_2. Indeed, we see that O_2 increases slightly later than O. During the long relaxation time after the gas has passed the plasma column (i.e., after t_r), we observe a slow depletion of O and a formation of O_2 and O_3.

In the calculations presented above, we used a fixed value for the reduced electric field of 50 Td. The reduced electric field influences the EEDF, and consequently, the importance of different electron excitation processes. Lower values tend to favour the processes with low activation energy, such as excitation of the vibrational levels, whereas high values favour the processes with high activation energies, such as excitation of electronic levels and dissociation. The effect of the reduced electric field value on the excitation of CO_2 has been shown before[17, 26] by solving the Boltzmann equation with the CO_2 ground state cross sections. In the present work, we have calculated how the reduced electric field and the corresponding change in the electron excitation influences the macroscopic conversion and energy efficiency; see figure 4. Moreover, from the reaction rates averaged over the whole simulation, we have also calculated the fraction of electron energy transferred to different excitation channels, which is also illustrated in figure 4. Our results are in good agreement with the previous calculations, showing that the asymmetric mode levels of CO_2 are best excited at a reduced electric field around 50 Td. Below 20 Td, the excitation of the symmetric mode levels becomes strongly dominant and the conversion and energy efficiency are practically zero. The energy efficiency curve clearly correlates with the energy supplied into the asymmetric mode levels, but the maximum is observed at a higher value of 70 Td. For E/N higher than 50 Td the energy loss due to excitation of electronic states increases, and it contributes even 50 % at 200 Td. Due to this, for E/N higher than 100 Td, the overall energy efficiency becomes less than optimal. Finally, it is interesting that the contribution of energy losses due to other processes (mainly dissociation, ionization, and excitation of reaction products) is always below 10 % in the E/N range examined.

Besides varying the specific energy input and the reduced electric field, we have also investigated the effect of the electron density on the CO_2 conversion and energy efficiency. An increase in the electron density means a proportional increase in the total power absorbed by the electrons (cf. equation (8)). That is why the residence time, t_r, needed to obtain the same SEI, is decreasing with an increasing electron density. As already discussed before, with the E/N constant, the residence time is approximately inversely proportional to the electron density, see equation (8). This is indeed observed in our simulation results, see the blue line and crosses in figure 5. The CO_2 conversion and energy efficiency (which are proportional to each other due to the fixed SEI, and therefore shown by a single curve) increase monotonically with increasing electron density. This is in agreement with the results obtained by Fridman using a one-temperature model [17] and can be explained by the competition between electron impact excitation and VT relaxation for population and depopulation of the CO_2 vibrational levels, respectively. In a simplified way, this can be evaluated by the characteristic time for vibrational excitation and by the characteristic time for vibrational relaxation τ_{VT}. The model, taking into account the densities of all vibrational levels and the state-to-state rate constants, can describe this very accurately. However, as a rough approximation, we can also estimate the characteristic time for VT relaxation as $\tau_{VT} \approx (k^{VT}_{1\to0}(T_{g0})N(T_{g0}))^{-1}$, where $k^{VT}_{1\to0}$ is the rate constant for VT relaxation of the CO_2v_1 level (see reaction (V2) in table A2),

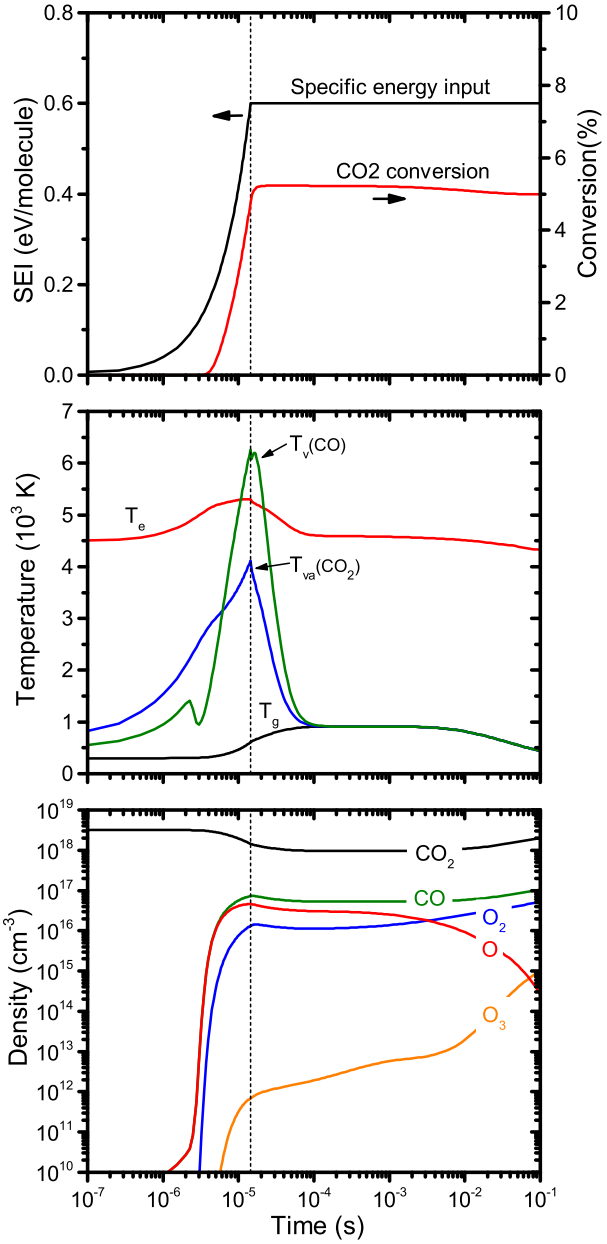

Figure 3. Time dependent analysis of the simulated discharge at $p = 100\,\mathrm{Torr}$, $E/N = 50\,\mathrm{Td}$, $n_\mathrm{e} = 10^{13}\,\mathrm{cm}^{-3}$ and SEI $= 0.6\,\mathrm{eV/molecule}$. The top panel shows the specific energy input (black line) and the CO_2 conversion (red line). The middle panel shows the time evolution of the gas temperature, T_g, the electron temperature, T_e, the vibrational temperature of the asymmetric mode of CO_2, $T_\mathrm{va}(CO_2)$, and the vibrational temperature of CO, $T_\mathrm{v}(CO)$. The bottom panel shows the densities of the most important neutral species. The residence time of the gas within the plasma column, i.e., $1.4 \times 10^{-5}\,\mathrm{s}$, is indicated by the vertical dashed line.

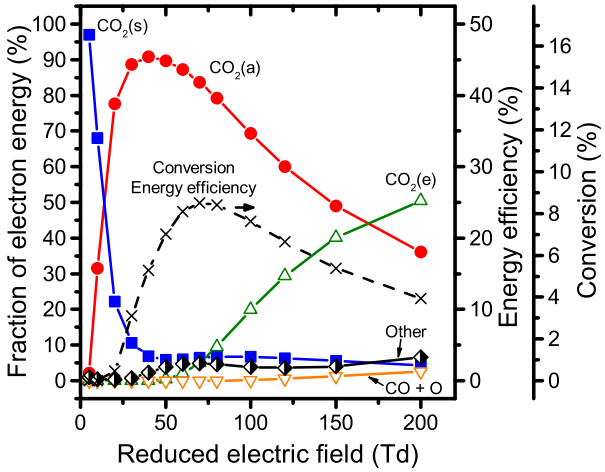

Figure 4. CO_2 conversion and energy efficiency as well as fraction of the electron energy lost in various reactions, as a function of the reduced electric field, E/N, calculated with $n_e = 10^{13}\,\mathrm{cm}^{-3}$ and SEI = 1.0 eV/molecule. Here, "CO_2(s)" represents vibrational excitation to all symmetric mode levels of CO_2, "CO_2(a)" represents vibrational excitation to all asymmetric mode levels of CO_2, "CO_2(e)" represents excitation of electronic levels of CO_2, "CO + O" corresponds to the electron impact dissociation of CO_2 and "Other" represents all other processes that make the complement to 100 %, e.g., ionization of CO_2 and all excitations and ionizations of dissociation products, most importantly CO, O_2 and O.

N is the gas density, and T_{g0} is the initial gas temperature. This yields $\tau_{VT} \approx 10^{-4}\,\mathrm{s}$ at a gas pressure of 100 Torr. Furthermore, the residence time of the gas within the plasma column, t_r, serves as a good estimate for the characteristic time of vibrational excitation.

When $t_r < \tau_{VT}$, i.e. excitation is faster than relaxation, we may obtain high enough densities of the excited levels that enable dissociation of the molecule. However, when $t_r > \tau_{VT}$, the density of the highly excited vibrational levels will be low due to their continuous relaxation. Figure 5 shows that in our case, when the gas temperature is self-consistently calculated in the model, we are unable to convert any CO_2 when the electron density is below $10^{12}\,\mathrm{cm}^{-3}$ (full red circles), or in other words, when the residence time is slightly longer than the estimated τ_{VT}. For higher electron densities, t_r becomes much shorter than τ_{VT} and the energy efficiency increases.

It is also important to take into account the effect of the gas temperature. The VT relaxation rate constants increase strongly with temperature, that is why we obtain a higher energy efficiency when the gas temperature is fixed at 300 K (empty red circles in figure 5) and the conversion starts to increase at a lower electron density threshold

Finally, figure 5 illustrates that for electron densities higher than $10^{14}\,\mathrm{cm}^{-3}$, the energy efficiency is practically saturated. This suggests that at this point, the energy efficiency is limited by the dissociation mechanism, i.e. the energy losses associated with the CO_2 splitting, rather than the VT relaxation.

Due to the relatively short time for VT relaxation at a pressure of 100 Torr, the residence time must be very short and consequently the electron density very high, to maximize the energy efficiency. For the highest values of the energy efficiency, the residence time seems to be too short (i.e., order of $10^{-6}\,\mathrm{s}$) to be realized in subsonic

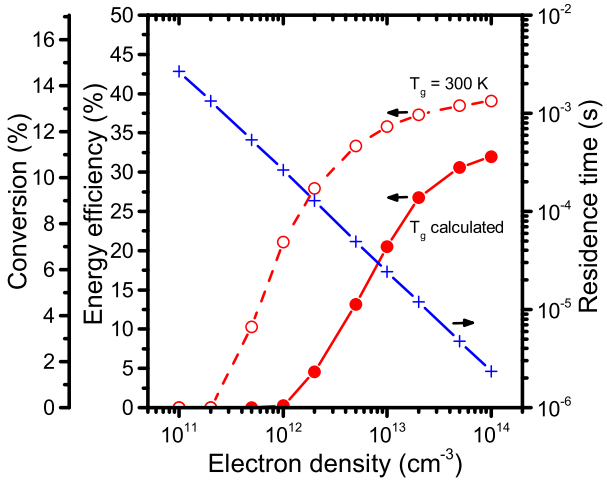

Figure 5. CO_2 conversion and energy efficiency as a function of the electron density, calculated for $p = 100$ Torr, $E/N = 50$ Td and SEI $= 1.0$ eV/molecule, for a fixed gas temperature of 300 K and a gas temperature calculated self-consistently in the model (red curves; open and full circles, respectively. The residence time needed to obtain the same SEI, as a function of the electron density, is also shown (blue line and crosses, and right y-axis).

flow conditions. This corresponds to the fact, that in the search for the highest energy efficiency, discharges with supersonic flow were realized[6]. A solution would be to use a lower gas pressure that increases the VT relaxation time and allows for longer residence times. However, lower gas pressures are not very convenient for practical (industrial) applications of CO_2 conversion. Moreover, in reality the gas pressure influences both the reduced electric field and the electron density. It can be expected that the reduced electric field, E/N, will decrease with increasing gas pressure due to the N^{-1} dependence. As shown in figure 4, the reduced electric field has a relatively narrow range ($50 - 100$ Td) where the maximum energy efficiency was achieved. Therefore, we believe that the conversion at a different gas pressure would be largely influenced by the reduced electric field in the plasma. If its value falls out of the optimum range, the energy efficiency would be limited. An exact determination of this influence is not simple, and requires a self-consistent simulation which determines the relation between the electric field and the electron density in a steady-state discharge. Therefore, we can not give a clear advice towards the optimum gas pressure based on our simulations at this moment.

3.2. Time evolution of the gas temperature

The gas temperature is calculated by the energy conservation equation (2), as explained in section 2 above. The main contribution comes from the relaxation of vibrational levels and from the chemical reactions. In section 3.1, we have shown the difference in the conversion and energy efficiency between the case when the gas temperature is fixed and the self-consistently calculated gas temperature; see figures 2 and 5. Qualitatively, the dependence of the energy efficiency on the specific energy input and on the electron density are the same, but the quantitative results differ

significantly.

Figure 6 shows the time evolution of the gas density for the two already presented series of calculations, i.e. with a varying specific energy input (top panel) and with a varying electron density (bottom panel). As seen in the top panel, the maximum gas temperature obtained increases with the specific energy input. This is due to the increasing energy input into the CO_2 vibrational levels and the subsequent transfer of this energy into the translational degrees of freedom through VT relaxation. At around 10^{-4} s, the gas temperature stops increasing, which corresponds to the equalization of the translational and vibrational temperatures; cf. the middle panel of figure 3.

From the bottom panel of figure 6, it is obvious that the gas temperature evolution is strongly influenced by the residence time, which is inversely proportional to the electron density. For $n_e = 10^{11}\,cm^{-3}$ and the corresponding long residence time (order of 10^{-3} s), the VT relaxation reactions transfer almost all vibrational energy into translation energy, which leads to a relatively slow increase of the gas temperature but a high gas temperature peak. On the other hand, for $n_e = 10^{14}\,cm^{-3}$ and the corresponding short residence time ($\approx 2 \times 10^{-6}$ s), some of the vibrational energy is used for the dissociation of CO_2 and, consequently, less vibrational energy contributes to gas heating. As a result, the maximum gas temperature is lower than for the cases with lower electron densities.

The gas temperature calculated by the model is in reasonable agreement with experimental results obtained under similar conditions, to be more specific, a peak gas temperature around 1100 K for the SEI around 1 eV/molecule [5] or a gas temperature in the range between 800 and 1200 K (depending on the power input) reported recently by Silva et al.[10].

The gas temperature influences the vibrational relaxation reactions (table A2) as well as the neutral chemical reactions (table A3). The dominant influence observed in figures 2 and 5 (i.e., lower conversion and energy efficiency at higher gas temperature) comes from the strong temperature dependence of the VT relaxation reactions, see (N2) in table A2. The gas heating thus becomes a runaway mechanism – increase in the gas temperature leads to further increase of the VT relaxation rates. Therefore, the gas temperature increases "exponentially" until the gas heating sources diminish or are balanced by the heat losses to the walls; see the increase of gas temperature in figure 6.

On the other hand, it could be argued that an increase in the gas temperature leads to a higher equilibrium population of the vibrational levels and the rate constants for the CO_2 dissociation reactions also increase with the gas temperature. However, our simulations show that, under the conditions investigated, these effects are clearly compensated by the increase of the VT relaxation rates which are responsible for most of the vibrational energy losses (see more details in section 3.3).

In order to further evaluate the possible increase in conversion and energy efficiency by increasing the initial population of the vibrational levels as a result of heating the CO_2 before entering the reactor, we have carried out a series of calculations with the initial CO_2 temperature varying in the range $300 - 2000$ K. The initial population of CO_2 vibrational levels was set according to a Boltzmann distribution at the given temperature. The specific energy needed to preheat the gas was evaluated from thermodynamical data of CO_2[25], see table 3. This specific energy was added to the specific energy input by the plasma (SEI), which was again fixed at 1.0 eV/molecule, and the sum was then used to calculate the energy efficiency by (12). The results in figure 7 show that in the temperature range $300 - 900$ K, both

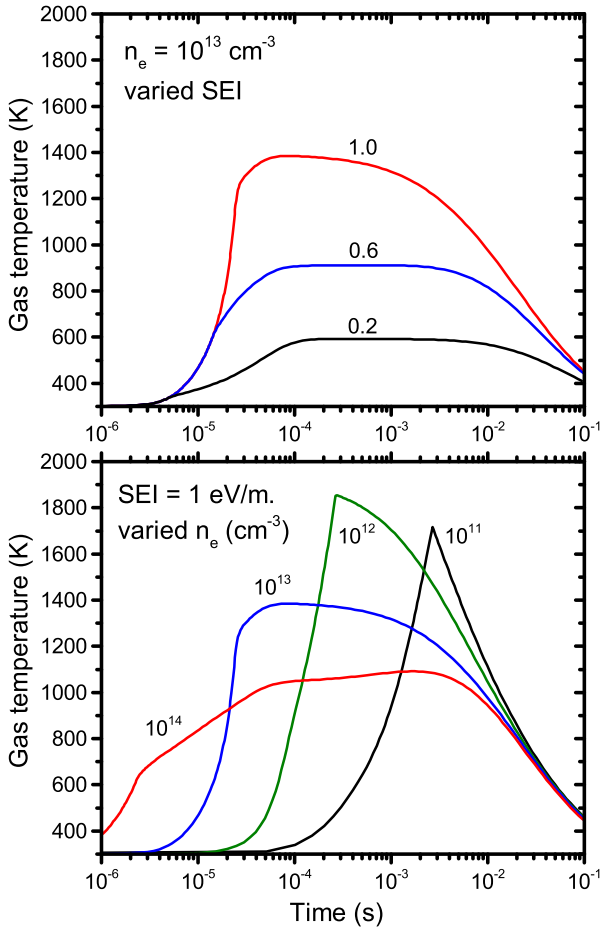

Figure 6. Time evolution of the gas temperature, calculated for $p = 100$ Torr, $E/N = 50$ Td and different values of the electron density and the specific energy input. In the top panel, $n_e = 10^{13}\,\mathrm{cm}^{-3}$, and the labels indicate the specific energy input. In the bottom panel, the specific energy input is fixed at 1.0 eV/molecule and the labels indicate the electron density.

the conversion and energy efficiency drop practically to zero with rising temperature, which can be explained by the increase in the VT relaxation rates, lowering the population of the high CO_2 vibrational levels that can give rise to dissociation. When the initial CO_2 temperature increases beyond 900, K, the conversion and energy efficiency increase again, but they reach practically the same values as obtained at 300 K only at the temperature of 2000 K. At this point, the conditions correspond practically to an equilibrium thermal plasma. The calculated peak gas temperature (due to further heating by the plasma) reaches 3400 K and the CO_2 vibrational temperature peaks at 3500 K. Therefore, the increased conversion compared to the result at 300 K is caused by the increase of the dissociation rates due to the increased gas temperature rather than by a more pronounced non-equilibrium population of the highly excited vibrational levels. It should be stressed out that at different conditions, especially at a different SEI, the conversion and energy efficiency values could be

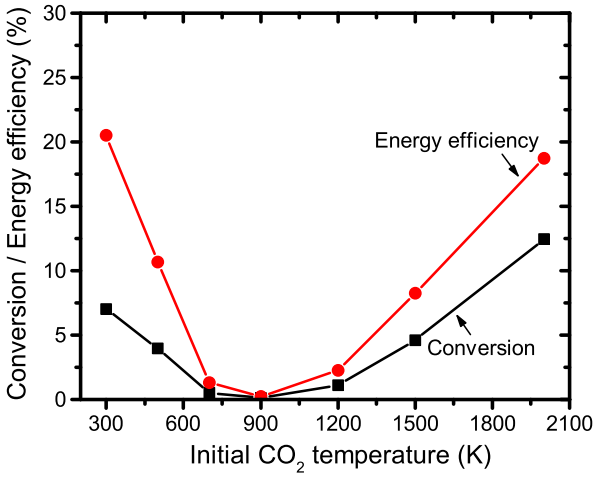

Figure 7. CO_2 conversion and energy efficiency as a function of the temperature of the CO_2 gas entering the reactor, calculated for $p = 100$ Torr, $E/N = 50$ Td, $n_e = 10^{13}$ cm^{-3} and SEI = 1.0 eV/molecule. In this case, the total specific energy input used in (12) to calculate the energy efficiency is a sum of the SEI and the specific energy needed to heat CO_2 to the given initial temperature, which is evaluated in table 3.

Table 3. Specific energy needed to heat the CO_2 to a given temperature, starting from the reference temperature of 300 K; calculated from CO_2 thermodynamic data[25].

Temperature (K)	Specific energy (eV/molecule)
300	0.000
500	0.085
700	0.183
900	0.290
1200	0.460
1500	0.639
2000	0.947

significantly different. Nevertheless, figure 7 shows qualitatively a transition from a plasma with non-equilibrium population of CO_2 vibrational levels to a thermal plasma. In the former case, an increase of the gas temperature lowers the energy efficiency, whereas in the latter case, the energy efficiency increases. Although, the energy efficiency calculated by the model under the given conditions is practically equal in the two different regimes at 300 and 2000 K, it is believed that a non-equilibrium plasma can theoretically provide a higher energy efficiency. The limiting factors for the energy efficiency calculated by the model in the non-equilibrium plasma case are further discussed in the next section.

3.3. Analysis of the energy efficiency

As mentioned before, the energy efficiency values obtained in our calculations are lower than the maximum values reported in the literature, especially with respect to

Rusanov and Fridman (where values up to 80 % were reported)[5]. However, in more recent experiments, such high values have not yet been obtained. Recently, Goede et al.[9] presented energy efficiencies in the range $25-35$ % under very similar conditions (pressure of 200 mbar, tube radius of 1.3 cm and low $E/N \sim 10$ Td) with a decreasing energy efficiency when the SEI increases from 1 to 10 eV. This is in a very good qualitative agreement with our results. At the same time we have to note that an exact comparison of the energy efficiency between our results is problematic due to the fact that we have little information about the electron density and reduced electric field in the experimental discharge, not to mention the tangential injection of the gas into the reactor used in the experiments, which cannot be simulated by the present model. For a specific energy input of 1 eV/molecule and an increased power and gas flow rate, they achieved a maximum energy efficiency of up to 55 %. The increase of the power and gas flow rate lead to an increased electron density and a shorter residence time. Thus, these results are also in good agreement with the trends identified in our simulations. It seems likely that a high energy efficiency (above 50 %) can be achieved only for a carefully optimized experimental setup and discharge conditions, more specifically for a narrow range of E/N values and a sufficiently high gas flow rate.

For a different discharge conditions characterized by a low pressure (1 mbar) and high $E/N \sim 1000$ Td, Goede et al. obtained energy efficiencies around 10 % which were independent on the power input [9]. From a calculation using the same plasma conditions with a variable electron density, we also obtained energy efficiencies independent on the electron density with values around 5 %. This indicates that despite the simplifications of the model, it provides correct trends in a wide range of process conditions.

In our simulations, we have analyzed the rates of individual reactions and evaluated the importance of different processes. In contrast to the simulations of a dielectric barrier discharge[11], vibrational excitation is the dominant dissociation channel over electronic excitation or direct electron-impact dissociation under the conditions investigated in the present paper. This has been already indicated by figure 4. The calculated density of electronic excited states is very low (maximum in the order of $10^{15}\,\mathrm{cm}^{-3}$ for the highest E/N value of 200 Td) and their effect on the conversion of CO_2 is negligible. Therefore, we focus our attention to the CO_2 vibrational levels and the energy losses attributed to reactions of the vibrational levels. These are shown as fractions of the total vibrational energy input in figure 8, as a function of time, for three cases with a different electron density value; cf. figure 5. Note that the vertical dashed lines again indicate the residence time of the gas within the plasma column for each case (i.e, the residence time needed to obtain the same SEI is again inversely proportional to the electron density values).

The role of the residence time and the characteristic time for VT relaxation (estimated to be in the order of 10^{-4} s), which has already been discussed before, is also perfectly illustrated in this figure. For an electron density of $10^{12}\,\mathrm{cm}^{-3}$ (top panel), VT relaxation consumes most of the vibrational energy put into CO_2. At the end of the simulation time, 90 % of the vibrational energy has been lost due to VT relaxation and 10 % due to VV' relaxation. Practically no vibrational energy has been used to dissociate the CO_2 molecules. This indeed corresponds to figure 5, where the conversion and energy efficiency are shown to be negligible at an electron density of $10^{12}\,\mathrm{cm}^{-3}$.

For the very high electron density of $10^{14}\,\mathrm{cm}^{-3}$ (bottom panel), the residence time

of 2.4×10^{-6} is significantly shorter than the characteristic time for VT relaxation. Consequently, the vibrational energy accumulated in CO_2 helps to dissociate the molecule through the processes D_M and D_O, which correspond to the two dissociation reactions (N1) and (N2) in table A3. Apart from VT and VV' relaxation, a small portion of the energy loss is due to VV relaxation, which is responsible for the step-by-step population of the high vibrational levels. During the relaxation phase ($t > t_r$), the remaining vibrational energy stored in the CO_2 and CO levels is relaxed mainly by the VT relaxation reactions whose fraction then increases up to 30 %. At the end of the simulation, 60 % of the vibrational energy has been used for dissociation of the CO_2 molecule, 30 % has been lost by VT relaxation and another 10 % by VV and VV' relaxation. This again corresponds well with figure 5, where the CO_2 conversion and energy efficiency are indeed at maximum (i.e., around 11 % and 32 %, respectively) at an electron density of $10^{14}\,\mathrm{cm}^{-3}$.

The middle panel shows the case with the electron density of $10^{13}\,\mathrm{cm}^{-3}$, which lies between the two extreme cases presented above. The results are qualitatively comparable to the case with the highest electron density, but more energy is lost by VT relaxation and, consequently, a slightly lower conversion and energy efficiency is obtained (cf. figure 5). Taking into account this dependence of the dissociation reactions D_M and D_O on the excitation and relaxation of the high lying asymmetric vibrational levels and the impact on the overall CO_2 conversion, we can clearly apreciate the importance of the vibrational levels in the conversion pathway. Without the high-lying vibrational levels of CO_2 in the model, the conversion would be practically zero under the same conditions.

As the density of CO increases with the conversion, a part of the CO_2 vibrational energy is transfered to the vibrational mode of CO due to the VV relaxation between both molecules; see the "VV_{CO}" label in the middle and bottom panel of figure 8. For $t > t_r$, there is no more new CO produced, and the fraction of energy lost due to VV relaxation and dissociation reactions remains constant. The remaining energy still stored in the vibrational levels of CO_2 (and also CO) starts to be consumed by VT relaxation; see its fraction increase after t_r. We can also notice that the fraction of VV_{CO} losses diminishes before the end of the simulation. This means that the vibrational energy is transferred from CO back to CO_2. This is a result of the fact that VT relaxation of CO_2 is faster than VT relaxation of CO, so the deficit of vibrational energy in CO_2 is compensated by VV transfer from CO, when available.

In the best case, we have used 60 % of the vibrational energy for dissociation of the CO_2 molecule (see bottom panel of figure 8, and this value is determined mainly by the rates of the CO_2 vibrational reactions (VV and VT relaxation) and the rate for the primary dissociation reaction (N1). However, even in this case, the energy efficiency is only around 32 % (see figure 5 above), hence much lower than this 60 %. In general, we must take into account that not all the input energy is used to excite the vibrational levels, although in this case it is as high as 95 %. More importantly, we have to examine whether the dissociation reactions correspond to the maximum possible CO_2 conversion. As we know, mainly two reactions, (N1) and (N2), also labeled D_M and D_O in figure 8, respectively, contribute to the CO_2 conversion. However, the theoretical maximum energy efficiency is achieved only when the ratio of their rates (D_O/D_M) is unity, which means that each oxygen atom produced by (N1) is used in (N2) to split another CO_2 molecule. Other processes, mainly oxygen recombination (N16), are consuming atomic oxygen, and thus competing with reaction (N2). Taking into account the reaction rates of the two dissociation reactions and the corresponding

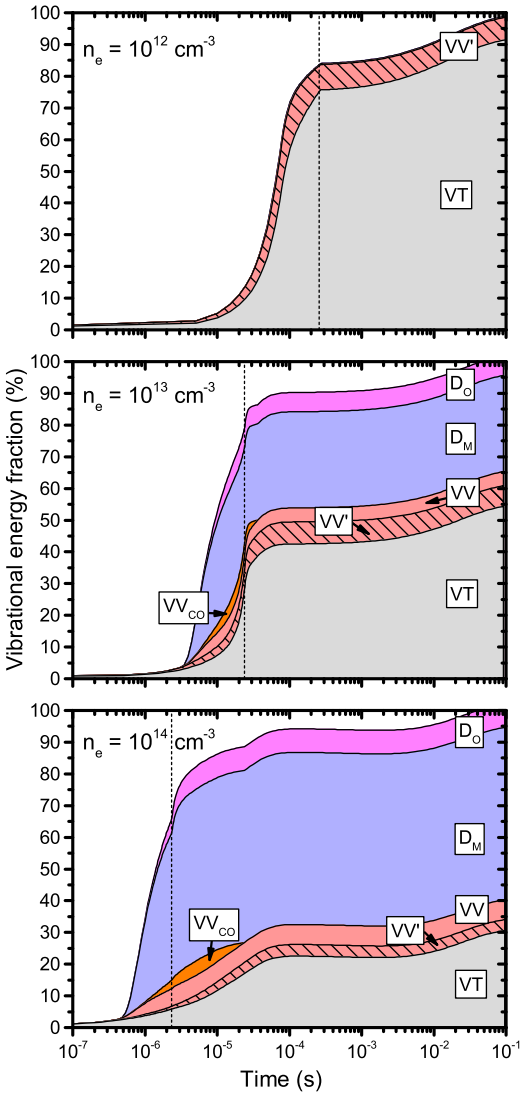

Figure 8. Fraction of the total CO_2 vibrational energy used by various processes. The results were obtained from simulations with $p = 100$ Torr, $E/N = 50$ Td and SEI $= 1.0$ eV/molecule, and for three different values of the electron denisty. The notation of the processes in this figure is as follows: "VT" corresponds to VT relaxation (reactions (V1) and (V2))), "VV"' corresponds to VV energy exchange between the asymmetric mode and symmetric mode CO_2 levels (reactions (V5)), "VV" represents VV relaxation among the asymmetric mode of CO_2 (reactions (V6)), "VV_{CO}" represents VV relaxation between CO_2 and CO molecules (reaction (V8)), "D_M" represents dissociation of CO_2 by reaction (N1), "D_O" represents dissociation of CO_2 by reaction (N2). The changes in energy gained or lost through individual processes are integrated in time, so for every moment in time, the figure represents the cumulative distribution of energy up to that moment.

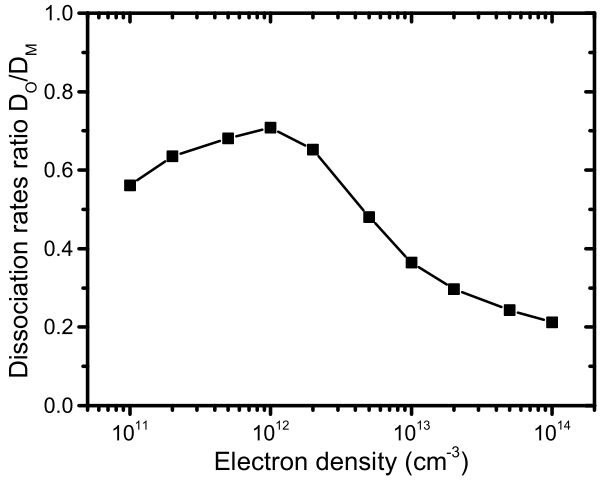

Figure 9. Ratio of rates for the CO_2 dissociation reactions D_O/D_M as a function of the electron density, where D_M is the dissociation by collision with an arbitrary molecule, reaction (N1), and D_O is the dissociation by reaction with atomic oxygen, reaction (N2). The simulation conditions were $p = 100\,\mathrm{Torr}$, $E/N = 50\,\mathrm{Td}$ and SEI $= 1.0\,\mathrm{eV/molecule}$. The rates were integrated during the entire simulation.

energy costs for the production of one CO molecule (see ΔH_r for (N1) and (N2) in table A3), we obtain the total energy cost for the production of one CO molecule as

$$\mathrm{CO\ cost\,(eV)} = \frac{5.52 + 0.35\, D_O/D_M}{1 + D_O/D_M}\,, \tag{14}$$

where D_O/D_M is the ratio of the rates of equations (N2) and (N1), respectively.

Figure 9 shows this ratio evaluated from the averaged rates in our simulations with the varying electron density. We can see that the ratio of the rates is around 0.6 when the electron density is lower than $10^{12}\,\mathrm{cm}^{-3}$ (but the conversion is practically zero at these conditions; cf. figure 5 above), but it decreases to 0.2 as the electron density increases to $10^{14}\,\mathrm{cm}^{-3}$; see figure 9. With the ratio of the dissociation rates equal to 0.2, the cost of producing a CO molecule becomes 4.66 eV instead of the theoretical minimum of 2.93 eV (see section 2.2 above), and thus our energy efficiency decreases by a factor of 1.6. To be more specific, in the case under discussion, 95 % of the energy is put into vibrations, of which 60 % is used for dissociation, which gives a theoretical maximum efficiency of 57 %. But, this has to be divided by 1.6 due to the low fraction of the (N2) reaction rate, which gives an efficiency of 36 %. The calculated energy efficiency of 32 % (cf. figure 5) is still slightly lower, but the most important limiting factors are thus identified in this way. The small difference is most likely due to vibrational energy losses in the reaction (N2), when a highly excited CO_2 molecule has a potential energy higher than needed to overcome the activation barrier. Then the excess vibrational energy is lost as the kinetic energy of the reaction products (at least it is assumed like that in the model).

To illustrate further that the dissociation reaction (N2) is limiting the energy efficiency, we have lowered the activation energy of this reaction from 1.43 eV to the theoretical minimum of 0.35 eV (equal to the enthalpy of the reaction). This

results in a higher rate constant (i.e. $1.2 \times 10^{-13}\,\mathrm{cm^3 s^{-1}}$ vs. $4.8 \times 10^{-19}\,\mathrm{cm^3 s^{-1}}$ at a gas temperature of 1000 K), to be more competitive with the oxygen recombination reaction (which is $3.1 \times 10^{-15}\,\mathrm{cm^3 s^{-1}}$ at the same gas temperature and a gas density (acting as third body) of $9.6 \times 10^{17}\,\mathrm{cm^{-3}}$, corresponding to the pressure of 100 Torr). Although this is an artificial correction, it should illustrate the sensitivity of the results to the reaction rate constants, which might be inaccurate. As pointed out by Fridman, the activation energy reported in the literature, which is typically determined through detailed balance from the inverse reaction, might be overestimated[27]. Figure 10 shows a comparison of the energy efficiency calculated with the original and the modified activation energy. As can be seen in the top panel, the maximum energy efficiency increases from 24 % to 38 % at the same specific energy input of 0.6 eV/molecule and an electron density of $10^{13}\,\mathrm{cm^{-3}}$. In the bottom panel, for the highest electron density of $10^{14}\,\mathrm{cm^{-3}}$, the energy efficiency reaches to 52 %. These values are thus comparable to the already mentioned highest values of Goede et al.[9]. The evaluation of the averaged dissociation rates showed that the ratio $D_\mathrm{O}/D_\mathrm{M}$ is equal to 1 in this case, demonstrating indeed that the theoretical maximum energy efficiency (taking into account the vibrational energy losses due to VT relaxation) is achieved only when each oxygen atom produced by (N1) is used in (N2) to split another CO_2 molecule.

We can summarize the discussion by pointing out that the energy efficiency of CO_2 conversion is mainly limited by three factors, (1) the amount of vibrational excitation of the CO_2 molecule, (2) the vibrational energy losses due to VT relaxation and (3) the oxygen radical chemistry, more specifically the way in which the produced atomic oxygen reacts to form either O_2 molecules or to split another CO_2 molecule. We have shown that the amount of vibrational excitation of the CO_2 molecule is optimal only in a narrow range of E/N. The vibrational energy losses due to VT relaxation will always be present, but they can be minimized by using a short residence time and by keeping the gas temperature low, which can be better realized at supersonic flow conditions.

Given the values of the energy efficiency obtained from the simulations even at the best case examined, when practically only the vibrational levels of the CO_2 are excited by the plasma electrons, and the residence time was very short, it seems that it is very difficult to obtain very high energy efficiencies (e.g. $> 60\,\%$) under experimental conditions, where more limitations, e.g. due to the power supply, gas flow, plasma instabilities etc., come into play. At this point, however, we should also remember the limitations of the model. They arise partly from the approximations necessary to use the zero-dimensional model and partly from the reaction chemistry used. With respect to the former, we should mention the assumed radial uniformity of all model variables and the corresponding approximations for gas velocity and thermal conductivity. With respect to the latter, it is worth mentioning that the reaction rate constants can be subject to large errors. We modelled only vibrational reactions with single-quantum transitions and the approximations used to determine the rate constants are in general less reliable for highly excited levels and elevated gas temperatures. Based on the low energy efficiencies obtained by the model compared to the known experimental and theoretical results, it seems that the VT relaxation rates used in the model might be overestimated. Certainly, more reliable data of the CO_2 vibrational interactions and the reactions of vibrationally excited molecules with other species are still needed by the modelling community. We think that the population of the high-energy levels (and thus the conversion) can also be increased by improving the description of the

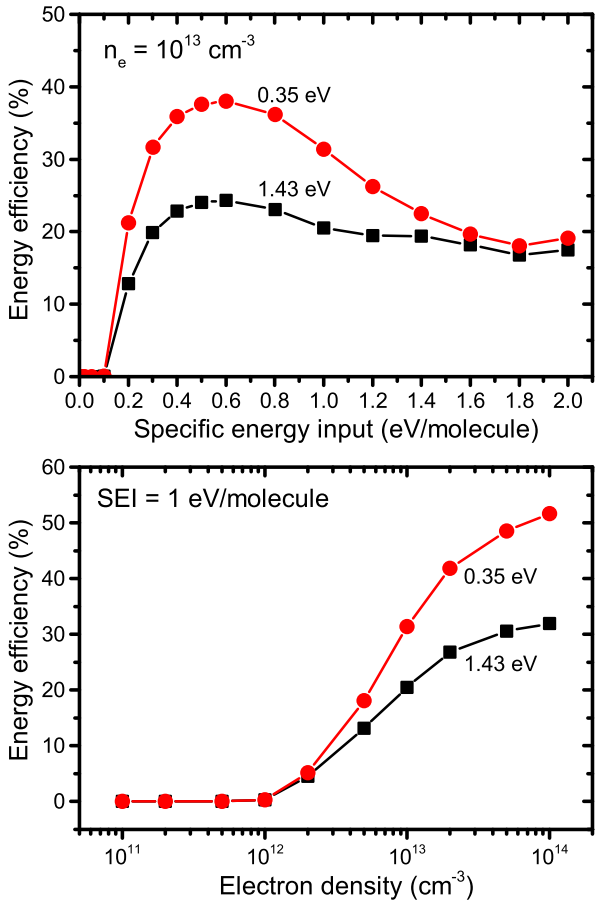

Figure 10. Influence of the value of the activation energy of the dissociation reaction $CO_2 + O \longrightarrow CO + O_2$ on the energy efficiency calculated by the model. The labels indicate the activation energy for the reaction used in the simulation. The value of 1.43 eV is the standard value used in all previous calculations, see table A3. The value of 0.35 eV is the theoretically minimum activation energy equal to the reaction enthalpy. The discharge conditions are $p = 100$ Torr, $E/N = 50$ Td, with the electron density and specific energy input value typeset in the figure panels.

symmetric mode vibrational levels, for example using a temperature-based model. We think that the complexity of the model would be too restrictive when symmetric mode levels are included as other species. A comparison of the present state-to-state model with a multi-temperature model for short-time-scale and long-time-scale processes would help us to find the optimal method to predict the CO_2 conversion in future models.

4. Conclusions

We have used a zero-dimensional reaction kinetics model to simulate CO_2 conversion in microwave discharges where the excitation of the vibrational levels plays a significant

role in the dissociation kinetics. The model implements a detailed description of the vibrational kinetics of the CO_2 and CO molecules. Moreover, a new aspect compared to our previous paper [11] is that the energy conservation equation for the gas temperature was solved together with the particle conservation equations.

The model was used to simulate a general tubular surfaguide microwave reactor, where a stream of CO_2 flows through a plasma column generated by microwave radiation. With respect to the necessary approximations which have been discussed, the model allows to study various discharge setups, differing in the reactor radius, gas pressure, gas flow rate etc. In this work, we have altered mainly the internal plasma parameters, namely the reduced electric field, electron density and the total specific energy input, and we studied their effects on the conversion and energy efficiency.

We have identified the discharge conditions that favour a high energy efficiency of the CO_2 conversion. The highest energy efficiency obtained in our calculations was around 32 %. To obtain this maximum energy efficiency, the specific energy input should be in the range $0.4 - 1.0\,\mathrm{eV/molecule}$ and the reduced electric field in the range $50 - 100\,\mathrm{Td}$. The energy efficiency increases with the electron density, which was explained by the competition between vibrational excitation and vibrational relaxation. When the specific energy input is fixed, an increase in the electron density leads to an increase in the energy deposition and a corresponding decrease of the residence time of the gas in the plasma. Thus, we have shown that a short residence time also favours a high energy efficiency, because the time for vibrational relaxation is longer than the residence time of the gas within the plasma column. This corresponds well with the fact, that the highest energy efficiencies were reported at supersonic flow conditions [6, 9].

Furthermore, to better understand the limitation in the energy efficiency, we have analyzed how the vibrational energy of CO_2 is used by individual reactions. Given the reaction set used in the model, we have seen that up to 60 % of the energy available in the CO_2 vibrational levels can be used for CO_2 dissociation, at least at high enough electron density (order of $10^{14}\,\mathrm{cm^{-3}}$ at the gas pressure of 100 Torr), corresponding to a short residence time of the gas within the plasma column (at the fixed SEI). The remaining fraction is largely consumed by VT relaxation which contributes to the gas heating. At lower electron densities, the fraction of energy consumed by VT relaxation becomes significantly larger, leading to a lower energy efficiency.

The gas temperature calculated by the model reaches peak values up to 1800 K for high energy inputs, but in calculations with the highest energy efficiency, it was typically around 1200 K. Because of the strong temperature dependence of the VT relaxation rates on the gas temperature, it is desirable to keep the gas temperature as low as possible to minimize the vibrational energy losses through VT relaxation. A higher gas temperature in principle also leads to an increased population of the vibrational levels and higher dissociation rates, but we have shown, that these effects are clearly compensated by the increased VT relaxation rates (and therefore lower energy efficiencies were obtained) in the temperature range from 300 K to around 1500 K. For even higher gas temperatures, the plasma is practically in thermal equilibrium and the energy efficiency increases with an increasing gas temperature, but in this regime, the advantages of non-equilibrium vibrational excitation of CO_2 are suppressed.

Finally, the energy efficiency is strongly influenced by the reaction chemistry of the atomic oxygen produced in the CO_2 dissociation reaction $CO_2 + M \longrightarrow CO + O + M$. When the atomic oxygen is not used further for dissociation through the reaction

$CO_2 + O \longrightarrow CO + O_2$, because it is lost by recombination into O_2 molecules, the theoretical energy efficiency further decreases. Given the rate constants obtained from the literature, we calculated an increase in the energy cost of a CO molecule up to a factor of 1.6, and hence a drop of 1.6 in the energy efficiency, due to this effect in our simulations. Hence, if the O atoms can be used selectively for further dissociation of the CO_2 molecules instead of recombining into O_2 molecules, the energy efficiency could be increased.

Qualitatively, the model predictions agree well with known experimental and theoretical results. Certainly, more accurate data for the vibrational kinetics of CO_2 would further improve the accuracy of the model predictions. A challenging next step would be to combine the reaction kinetics model with a more accurate simulation of the microwave discharge which would allow for a better comparison and validation with experiments.

Acknowledgments

This research has been funded by the Interuniversity Attraction Poles Programme initiated by the Belgian Science Policy Office, and by the Belgian Francqui organization. The calculations were carried out using the Turing HPC infrastructure at the CalcUA core facility of the Universiteit Antwerpen, a division of the Flemish Supercomputer Center VSC, funded by the Hercules Foundation, the Flemish Government (department EWI) and the Universiteit Antwerpen.

References

[1] 2007 *Fourth Assessment Report: Climate Change 2007 Synthesis Report* (IPCC: Geneva, Switzerland) URL `http://www.ipcc.ch/publications_and_data/ar4/syr/en/contents.html`
[2] Semiokhin I A, Andreev Y P and Panchenkov G M 1964 *Russ. J. Phys. Chem.* **38** 1126
[3] Maltsev A N, Eremin E N and Ivanter L V 1967 *Russ. J. Phys. Chem.* **41** 633
[4] Andreev Y P, Semiokhin I A, Voronkov Y M, Sirotkina V A and Kaigorodov V A 1971 *Russ. J. Phys. Chem.* **45** 1587
[5] Rusanov V D, Fridman A A and Sholin G V 1981 *Soviet Physics Uspekhi* **24** 447
[6] Asisov R I, Fridman A A, Givotov V K, Krasheninnikov E G, Petrushev B I, Potapkin B V, Rusanov V D, Krotov M F and Kurchatov I V 1981 Carbon dioxide dissociation in non-equilibrium plasma *5th International Symposium on Plasma Chemistry, Edinburgh* vol 2 p 774
[7] Spencer L F and Gallimore A D 2011 *Plasma Chem. Plasma Process.* **31**) 79
[8] Spencer L F and Gallimore A D 2013 *Plasma Sources Sci. Technol.* **22** 015019
[9] Goede A P H, Bongers W A, Graswinckel M F, van de Sanden R M C M, Leins M, Kopecki J, Schulz A and Walker M 2013 Production of solar fuels by CO_2 plasmolysis *3rd European Energy Conference, Budapest, Hundary*
[10] Silva T, Britun N, Godfroid T and Snyders R 2014 *Plasma Sources Sci. Technol.* **23** 025009
[11] Kozák T and Bogaerts A 2014 *Plasma Sources Sci. Technol.* **23** 045004
[12] Tannehill J C, Anderson D A and Pletcher R H 1997 *Computational fluid mechanics and heat transfer, 2nd ed.* (Taylor & Francis)
[13] Pancheshnyi S, Eismann B, Hagelaar G and Pitchford L Computer code zdplaskin URL `http://www.zdplaskin.laplace.univ-tlse.fr (University of Toulouse, LAPLACE, CNRS-UPS-INP, Toulouse, France, 2008)`
[14] Hagelaar G J M and Pitchford L C 2005 *Plasma Sources Sci. Technol.* **14** 722
[15] Guerra V, Tatarova E, Dias F M and Ferreira C M 2002 *J. Appl. Phys.* **91** 2648
[16] Vesovic V, Wakeham W A, Olchowy G A, Sengers J V, Watson J T R and Millat J 1990 *Journal of Physical and Chemical Reference Data* **19** 763
[17] Fridman A 2008 *Plasma Chemistry* (Cambridge University Press)
[18] Capitelli M, Colonna G, Pascale O D, Gorse C, Hassouni K and Longo S 2009 *Plasma Sources Science and Technology* **18** 014014

[19] Lawrence G M 1971 *Chem. Phys. Lett.* **9** 575
[20] Capitelli M, Ferreira C M, Gordiets B F and Osipov A I 2000 *Plasma Kinetics in Atmospheric Gases* (Springer)
[21] Laporta V, Cassidy C M, Tennyson J and Celiberto R 2012 *Plasma Sources Science and Technology* **21** 045005
[22] Treanor C E, Rich J W and Rehm R G 1968 *J. Chem. Phys.* **48** 1798
[23] Schwartz R N, Slawsky Z I and Herzfeld K F 1952 *The Journal of Chemical Physics* **20** 1591
[24] Levine R and Bernstein R 1976 Thermodynamic approach to collision processes *Dynamics of Molecular Collisions* (*Modern Theoretical Chemistry* vol 2) (Springer US)
[25] Chase M W J 1998 *J. Phys. Chem. Ref. Data, Monograph 9* 1
[26] Aerts R, Martens T and Bogaerts A 2012 *The Journal of Physical Chemistry C* **116** 23257
[27] Fridman A Solvay workshop on plasmas for environmental applications, 31st march - 2nd april 2014, brussels (private communication)
[28] Itikawa Y 2002 *J. Phys. Chem. Ref. Data* **31** 749
[29] Hayashi M 1990 Electron collision cross-sections determined from beam and swarm data by boltzmann analysis *Nonequilibrium Processes in Partially Ionized Gases* (*NATO ASI Series* vol 220) ed Capitelli M and Bardsley J (Springer US)
[30] Hayashi M 2003 *NIFS-DATA* **74**
[31] Land J E 1978 *J. Appl. Phys.* **49** 5716
[32] Mangan M A, Lindsay B G and Stebbings R F 2000 *J. Phys. B: At., Mol. Opt. Phys.* **33** 3225
[33] Janev R K and Reiter D 2003 *ChemInform* **34**
[34] Janev R, Wang J, Murakami I and Kato T 2001 *NIFS-DATA* **68**
[35] Phelps A V 1985 Tabulations of collision cross sections and calculated transport and reaction coefficients for electron collisions with o2, technical report 28 Tech. rep. JILA information center
[36] Krishnakumar E and Srivastava S 1992 *Int. J. Mass Spectrom. Ion Processes* **113** 1
[37] Liu C, Eliasson B, Xue B, Li Y and Wang Y 2001 *React. Kinet. Catal. Lett.* **74** 71
[38] Eliasson B and Kogelschatz U 1986 Basic data for modelling of electrical discharges in gases: Oxygen Tech. rep. Brown Boveri Research Report KLR 86-11C
[39] Matejcik S, Kiendler A, Cicman P, Skalny J, Stampfli P, Illenberger E, Chu Y, Stamatovic A and Märk T D 1997 *Plasma Sources Sci. Technol.* **6** 140
[40] Itikawa Y and Ichimura A 1990 *J. Phys. Chem. Ref. Data* **19** 637
[41] Laher R R and Gilmore F R 1990 *J. Phys. Chem. Ref. Data* **19** 277
[42] Blauer J A and Nickerson G R 1973 A survey of vibrational relaxation rate data for processes important to CO2-N2-H2O infrared plume radiation Technical report afrpl-tr-73-57 Ultrasystems, Inc.
[43] Kreutz T G, O'Neill J A and Flynn G W 1987 *The Journal of Physical Chemistry* **91** 5540
[44] Sharma R D 1969 *Phys. Rev.* **177** 102
[45] Cenian A, Chernukho A, Borodin V and Śliwiński G 1994 *Contrib. Plasma Phys.* **34** 25
[46] Cenian A, Chernukho A and Borodin V 1995 *Contrib. to Plasma Phys.* **35** 273
[47] Beuthe T G and Chang J S 1997 *Japanese Journal of Applied Physics* **36** 4997
[48] Mick H J, Burmeister M and Roth P 1993 *AIAA Journal* **31** 671
[49] Kossyi I A, Kostinsky A Y, Matveyev A A and Silakov V P 1992 *Plasma Sources Sci. Technol.* **1** 207
[50] Hadj-Ziane S, Held B, Pignolet P, Peyrous R and Coste C 1992 *J. Phys. D: Appl. Phys.* **25** 677

Appendix A. List of chemical reactions in the model

Table A1. Electron impact reactions described by collision cross sections.

No.	Reaction	Ref.	Note
(X1)	$e + CO_2 \longrightarrow e + CO_2$	[28]	a
(X2)	$e + CO_2 \longrightarrow e + e + CO_2^+$	[28]	a
(X3)	$e + CO_2 \longrightarrow e + e + CO^+ + O$	[28]	b
(X4)	$e + CO_2 \longrightarrow e + e + C^+ + O_2$	[28]	b
(X5)	$e + CO_2 \longrightarrow e + e + O^+ + CO$	[28]	b
(X7)	$e + CO_2 \longrightarrow O^- + CO$	[28]	b
(X8)	$e + CO_2 \longrightarrow e + CO + O$	[28]	b
(X9)	$e + CO_2 \longrightarrow e + CO_2e_1$	[29]	a
(X10)	$e + CO_2 \longrightarrow e + CO_2e_2$	[29]	a
(X11)	$e + CO_2 \longrightarrow e + CO_2v_a$	[30]	
(X12)	$e + CO_2 \longrightarrow e + CO_2v_b$	[30]	
(X13)	$e + CO_2 \longrightarrow e + CO_2v_c$	[30]	
(X14)	$e + CO_2 \longrightarrow e + CO_2v_d$	[30]	
(X15)	$e + CO_2v_i \longrightarrow e + CO_2v_j$	[30]	c
(X16)	$e + CO \longrightarrow e + CO$	[31]	a
(X17)	$e + CO \longrightarrow e + e + CO^+$	[31, 32]	a
(X18)	$e + CO \longrightarrow e + e + C^+ + O$	[31, 32]	b
(X19)	$e + CO \longrightarrow e + e + C + O^+$	[31, 32]	b
(X20)	$e + CO \longrightarrow C + O^-$	[31]	b
(X21)	$e + CO \longrightarrow e + COe_1$	[31]	a
(X22)	$e + CO \longrightarrow e + COe_2$	[31]	a
(X23)	$e + CO \longrightarrow e + COe_3$	[31]	a
(X24)	$e + CO \longrightarrow e + COe_4$	[31]	a
(X25)	$e + COv_i \longrightarrow e + COv_j$	[31]	d
(X26)	$e + C \longrightarrow e + C$	[33]	
(X27)	$e + C \longrightarrow e + e + C^+$	[33]	
(X28)	$e + C_2 \longrightarrow e + C_2$	[34]	
(X29)	$e + C_2 \longrightarrow e + C + C$	[34]	
(X30)	$e + C_2 \longrightarrow e + e + C_2^+$	[34]	
(X31)	$e + O_2 \longrightarrow e + O_2$	[35]	a
(X32)	$e + O_2 \longrightarrow e + O + O$	[35]	b
(X33)	$e + O_2 \longrightarrow e + e + O_2^+$	[35]	a
(X34)	$e + O_2 \longrightarrow e + e + O + O^+$	[36]	b
(X35)	$e + O_2 \longrightarrow O^- + O$	[35]	b
(X36)	$e + O_2 \longrightarrow e + O_2v_i$	[35]	
(X37)	$e + O_2 \longrightarrow e + O_2e_1$	[35]	
(X38)	$e + O_2 \longrightarrow e + O_2e_2$	[35]	
(X39)	$e + O_3 \longrightarrow e + O_3$	[37]	
(X40)	$e + O_3 \longrightarrow e + O_2 + O$	[38]	
(X41)	$e + O_3 \longrightarrow e + e + O_2^+ + O$	[38]	
(X42)	$e + O_3 \longrightarrow e + O^+ + O^- + O$	[38]	
(X43)	$e + O_3 \longrightarrow O^- + O_2$	[39]	
(X44)	$e + O_3 \longrightarrow O + O_2^-$	[39]	
(X45)	$e + O^- \longrightarrow e + O$	[40]	
(X46)	$e + O \longrightarrow e + e + O^+$	[41]	

(a) Same cross section used for reactions of CO_2v_i, and analogously for COv_i or O_2v_i.
(b) Cross section modified by lowering the energy threshold by the excited state energy used for reactions of CO_2v_i, and analogously for COv_i and O_2v_i.
(c) Cross section $0 \rightarrow 1$ scaled and shifted using Fridman's approximation[11].
(d) Cross sections $0 \rightarrow j$ ($j = 1 \ldots 10$) scaled and shifted using Fridman's approximation[11].

Table A2. Vibrational energy transfer reactions of CO_2, CO and O_2.

No.	Reaction	Rate constant ($cm^3 s^{-1}$); forward, $i = 1$	Ref.	Note
(V1)	$CO_2v_x + M \longleftrightarrow CO_2 + M$	$7.14 \times 10^{-8} \exp(-177T_g^{-1/3} + 451T_g^{-2/3})$	[42]	x=a,b,c,d
(V2a)	$CO_2v_i + M \longleftrightarrow CO_2v_{i\text{-}1(a)} + M$	$0.43 \exp(-407T_g^{-1/3} + 824T_g^{-2/3})$	[42]	
(V2b)	$CO_2v_i + M \longleftrightarrow CO_2v_{i\text{-}1(b)} + M$	$0.86 \exp(-404T_g^{-1/3} + 1096T_g^{-2/3})$	[42]	
(V2c)	$CO_2v_i + M \longleftrightarrow CO_2v_{i\text{-}1(c)} + M$	$1.43 \times 10^{-5} \exp(-252T_g^{-1/3} + 685T_g^{-2/3})$	[42]	
(V3)	$COv_i + M \longleftrightarrow COv_{i\text{-}1} + M$	$8.84 \times 10^{-12} T_g \exp(-222T_g^{-1/3} + 379T_g^{-2/3})$	[20]	
(V4)	$O_2v_i + M \longleftrightarrow O_2v_{i\text{-}1} + M$	$7.99 \times 10^{-5} \exp(-320T_g^{-1/3} + 615T_g^{-2/3})$	[42]	
(V5)	$CO_2v_i + CO_2 \longleftrightarrow CO_2v_{i\text{-}1} + CO_2v_x$	$2.13 \times 10^{-5} \exp(-242T_g^{-1/3} + 633T_g^{-2/3})$	[42]	x=a,b
(V6)	$CO_2v_i + CO_2v_j \longleftrightarrow CO_2v_{i\text{-}1} + CO_2v_{j+1}$	$1.8 \times 10^{-11} \exp(24.7T_g^{-1/3} - 65.7T_g^{-2/3})$	[43, 44]	$j = 1$
(V7)	$COv_i + COv_j \longleftrightarrow COv_{i\text{-}1} + COv_{j+1}$	$1.5 \times 10^{-15} T_g \exp(1.97T_g^{-1/3} + 82.3T_g^{-2/3})$	[20]	$j = 1$
(V8)	$CO_2v_i + COv_j \longleftrightarrow CO_2v_{i\text{-}1} + COv_{j+1}$	$4.8 \times 10^{-12} \exp(10^{-6}T_g^{-1/3} - 153T_g^{-2/3})$	[42]	$j = 0$

Table A3. Reactions of neutrals included in the model. In the rate constant expressions, T_g is the translational gas temperature in K. The rate constants are in $cm^3 s^{-1}$ or $cm^6 s^{-1}$ for binary or ternary reactions, respectively. The heat released in the reaction (in eV) is specified by ΔH_r. The α parameter determines the effectiveness of lowering the activation energy for reactions of vibrationally excited levels of CO_2, CO and O_2.

No.	Reaction	Rate constant	ΔH_r (eV)	α	Ref.
(N1)	$CO_2 + M \longrightarrow CO + O + M$	$4.39 \times 10^{-7} \exp(-65000/T_g)$	-5.52	1.0	[17]
(N2)	$CO_2 + O \longrightarrow CO + O_2$	$7.77 \times 10^{-12} \exp(-16600/T_g)$	-0.35	0.5	[17]
(N3)	$CO + O + M \longrightarrow CO_2 + M$	$8.2 \times 10^{-34} \exp(-1510/T_g)$	5.52	0.0	[45]
(N4)	$O_2 + CO \longrightarrow CO_2 + O$	$1.23 \times 10^{-12} \exp(-12800/T_g)$	0.35	0.5	[17]
(N5)	$CO_2 + C \longrightarrow CO + CO$	1.0×10^{-15}	5.64		[46]
(N6)	$CO + O_3 \longrightarrow CO_2 + O_2$	4.0×10^{-25}	4.41		[47]
(N7)	$CO + C + M \longrightarrow C_2O + M$	6.5×10^{-32}			[45]
(N8)	$O_2 + C \longrightarrow CO + O$	3.0×10^{-11}	5.99		[45]
(N9)	$CO + M \longrightarrow O + C + M$	$1.52 \times 10^{-4} (T_g/298)^{-3.1} \exp(-129000/T_g)$	-11.16	1.0	[48]
(N10)	$O + C + M \longrightarrow CO + M$	$2.14 \times 10^{-29} (T_g/300)^{-3.08} \exp(-2114/T_g)$	11.16		[47]
(N11)	$O + C_2O \longrightarrow CO + CO$	5.0×10^{-11}			[46]
(N12)	$O_2 + C_2O \longrightarrow CO_2 + CO$	3.3×10^{-13}			[45]
(N13)	$O + O_3 \longrightarrow O_2 + O_2$	$3.1 \times 10^{-14} T_g^{0.75} \exp(-1575/T_g)$	4.06		[45]
(N14)	$O_3 + M \longrightarrow O_2 + O + M$	$4.12 \times 10^{-10} \exp(-11430/T_g)$	-1.10		[47]
(N15)	$O + O_2 + M \longrightarrow O_3 + M$	$6.11 \times 10^{-34} (T_g/300)^{-2.6}$	1.10		[49]
(N16)	$O + O + M \longrightarrow O_2 + M$	$1.27 \times 10^{-32} (T_g/300)^{-1} \exp(-170/T_g)$	5.17		[50]